한국소음진동공학회 2003년도 춘계학술대회논문집, pp. 762~769.

초소형 광디스크 드라이브용 압전형 액츄에이터 제작

A Slim PZT Actuator for Small form Factor Optical Disk Drives

양우성*·이승엽**·박영필***

Woosung Yang, Seung-Yop Lee and Young-Phil Park

Key Words : Multi-layer Bimorph PZT(적층형 압전소자), Actuator(구동기), Flexure Hinge (유연 힌지), ODD(광디스크 드라이브), Pickup Actuator(픽업 구동기), Euler Beam(오일러 보), Timoshenko Beam(티모센코 보)

ABSTRACT

본 연구에서는 적층형 압전소자를 이용하여 초소형 및 슬림형 광디스크 드라이브용 광픽업 구동기를 개발하였다. 최근에 휴대용 정보기기의 급격한 발달로 인해 다양한 형태의 초소형 정보저장기기가 사용되고 있으며 착탈식 형태의 초소형 광디스크를 사용하는 ODD 가 개발 중에 있다. 적층 형태의 압전소자와 유연 힌지 형태의 변위 확대기구를 사용하여 구동기의 출력 힘과 허용 변위를 증가시키도록 설계하였다. 압전형 구동기의 동특성을 고려한 모델링과 이론적 해석을 통해 목표 변위와 성능을 만족하도록 설계 변수를 최적화하였고 이를 ANSYS 를 이용한 해석과 비교하였다. 상용화된 적층형 압전소자를 이용한 prototype 을 제작하여 실험을 수행하였으며 이론적인 예상 값과 잘 일치함을 보였다. 이와 같은 이론적 해석과 실험 결과를 토대로 높이가 2.5 mm 이며 15V 에서 $\pm 400\mu m$ 의 변위를 갖는 슬림형 및 초소형 ODD 에 적합한 압전형 구동기를 설계하였다.

1. Introduction

During the past few years, optical data recording devices are widely used by the developments of various information devices. Recent trends in optical disk drives are the development of small form factor ODDs for mobile devices, the spread of various rewritable DVD disk drives and the advent of BD/AOD drives, new high density ODDs which can store a HDTV movie.

The demand of slim-type optical disk drives has been dramatically increased for growing notebook market. Recently, small form factor (SFF) ODDs have been studied by several drive companies. The disk size would be similar to that of a IBM microdrive in HDD. The demand for size reduction in both the slim-type and SFF ODDs will be one of the most critical issues to overcome.

Piezoelectric actuators are considered as alternative to replace the conventional optical pick-up for small size ODDs. PZT materials show the fast response, easy miniaturization, good dynamic performance, however the low resultant force and displacement for high input voltages would prevent the application to ODD actuators.

In this paper, we propose a small size pick-up actuator using a bimorph multi-layer PZT for the application of slim and small form factor ODDs. A theoretical model, including dynamics of multi-layer PZT is derived and it is analytically solved to predict the natural frequency and the resultant force and displacement of the PZT actuator. A flexure hinge mechanism is used as displacement amplifier to extend the allowable stroke. The prototype of proposed model was manufactured using commercial bimorph PZTs. Experimental results agrees well with the analytical predictions. Based on the theoretical analysis and the preliminary experiments, we propose a final model for a new PZT pick-up actuator with 2.5-mm height, which can be applicable to small form factor optical disk drives.

* 서강대학교 기계공학과 대학원
E-mail : dreamrize@sogang.ac.kr
Tel : (02) 706-8280, Fax : (02) 712-0799
** 서강대학교 기계공학과, 정회원
*** 연세대학교 기계공학과, 정회원

2. Modeling of the bimorph multi-layer PZT actuator

Piezoelectric actuators usually take two kinds of PZT configurations, either stacked or bimorph. The stacked piezoelectric actuators with a simple structure generate a large force output. However, they require high voltages to operate and do not have a small displacement stroke. Therefore, bimorph piezoelectric actuators are used in the cases where large displacements and low applied voltage are needed,

The bimorph type actuator can operate by low voltages, but the resultant force generated at the edge of the actuator beam is not enough. It also has a shortcoming of low natural frequency. The PZT actuators with several bimorph layers can enlarge both the output force and the natural frequency, even though driving voltages are increased. Design variables associated with the PZT actuators should be properly selected for optimal performance. Thus, in this section, we consider the theoretical modeling and analysis for the multi-layer bimorph bending PZT actuator.

2.1 Static analysis of the bimorph PZT actuator

In general, a bimorph PZT actuator is bonded to the top and bottom surfaces of the structures and it is driven by voltages of the opposite polarity. Therefore, when one is expanded, the other is contracted. As shown in Fig. 1, the electrode and substrate layers exist between two adjacent PZT layers. t_{PZT} and t_{stru} are the thickness of the piezoelectric and connection layers, respectively. b is the layer width. Usually a bimorph PZT multi-layer has a symmetry structure in the x direction. We suppose that the total thickness of the PZT actuator is small enough for slander beam analysis where only the strain (ε_{PZT}) of x direction exists.

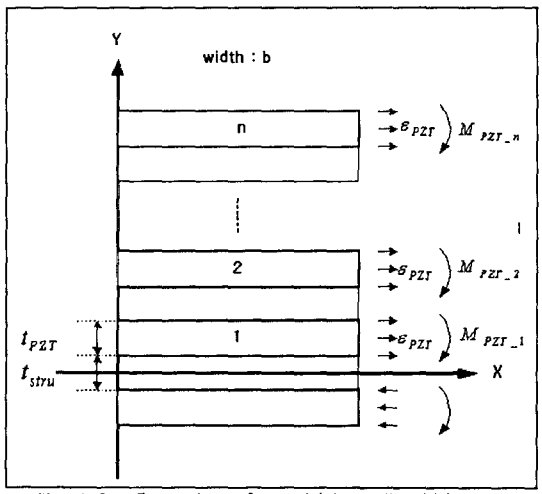

Fig. 1 Configuration of a multi-layer PZT bimorph bending beam actuator

The constituent equation of a piezoelectric material is expressed as

$$S = s_E T + dE$$
$$D = dT + \varepsilon_T E \quad (1)$$

Here s_E is the compliance at E=0 and ε_T is the relative dielectric at T=0) Also, if the thickness of a PZT layer is smaller than that of all the layers, the electric field impressed inside the PZT layer can be also approximated as

$$\varepsilon_{PZT} = d_{31}\frac{V_{in}}{t_{PZT}} \quad (2)$$

Here d_{ij} is the PZT coupling, V_{in} is the applied voltage, and t is the layer thickness. In this analysis, we take the following assumptions: (a) beam is modeled as slander beam with pure bending, (b) xz plane is the plane of symmetry, (c) xy plane is the neutral surface, (d) plane sections remain the same plane $\gamma_{xy} = \gamma_{xz} = 0$, (e) equilibrium requires that the resultant of the stress distribution over the cross section of the beam should equal the bending moment M_{PZT},

$$\sum M_y = \int_A z\sigma_x dA = M_{PZT}$$

The PZT elements are bonded to or embedded in a passive base structure. Here we consider one dimensional beam structure attached to the PZT. In each structure, we assume that the stacked beam is perfectly bonded so that the linear motion is generated at the interface. Then we can apply the conventional assumptions on stress and strain distributions to this analysis.

2.1 Analysis of bimorph three-layer PZT actuator

The strain that produces stress in the PZT is the superposition of the PZT strain (free strain, ε_{PZT}) and the bending strain (ε_{stru}). The PZT elements exert a distributed moment on the beam. Here we find a relation between the moment per unit length and the free strain. The strain equation at the joint of the PZT and connection layers is expressed as

$$\varepsilon_{act\_i} = \varepsilon_{stru\_i} - \varepsilon_{PZT} \quad (3)$$

Here the subscript i indicates the i-th layer. The moments about the neutral axis due to the resultant stress must balance such as

$$\int_0^{t_{stru}} \sigma_{stru} bzdz + \int_{t_{stru}}^{t_{stru}+t_{act}} \sigma_{act} badz = 0 \quad , \quad (4)$$

where $$\sigma_{stru} = \sigma_{stru\_i}\frac{z}{t_{stru}} \quad (5)$$

Substitution of Eqs. (3) and (5) into Eq. (4) gives

$$\sigma_{stru\_i} = K\sigma_{act\_i} \quad , \quad (6)$$

where $$K = \frac{-3t_{stru}t_{act}(2t_{stru}+t_{act})}{2(t_{stru}^3 + E_R t_{act}^3) + 3E_R t_{stru} t_{act}^2}, E_R = \frac{E_{act}}{E_{stru}} \quad (7)$$

The Hooke's law gives the following the stress-strain relations

$$\sigma_{stru\_i} = E_{stru}\varepsilon_{stru\_i}, \sigma_{act\_i} = E_{act}(\varepsilon_{stru\_i} - \varepsilon_{PZT}) \quad (8)$$

And the following expression is given by [1]

$$\therefore \varepsilon_{stru\_i} = \frac{-KE_R}{1-KE_R}\varepsilon_{PZT} \quad (9)$$

The moment M that is generated by the PZT layer, is

represented as

$$M = M_y = \frac{2}{3} M_{act} \tag{10}$$

Here, M_{act} is the moment that interacts in beam. The integration of stress over the sectional area of beam, gives

$$M_{act} = 2\int_0^{t_{stru}} \sigma_{stru\_i} bzdz = bt_{stru}{}^2 \sigma_{stru\_i}{}^2 \tag{11}$$

Using Eq. (11), the moment may be induced as following.

$$M = \frac{2}{3} bt_{stru}{}^2 E_{stru} \frac{-KE_R}{1-KE_R} d_{31} \frac{V}{t_{PZT}} \tag{12}$$

By Eq. (12), the maximum deflection at the edge of beam can be obtained when voltage is applied to the symmetric three (PZT-substrate-PZT) layers.

2.2 Analysis of bimorph multi-layer PZT actuator

If PZT is stacked to several layers, Eq. (12) is not valid because the moment is generated at each PZT layer. The total moment generated in the stacked beam structure can be calculated by the fact that strain (ε_{PZT}) of each PZT layer is constant. First of all, we assume $\sigma_y = \sigma_z = \tau_{yz} = 0$. The nonzero stress component is

$$\sigma_x = -E\frac{z}{\rho} \tag{13}$$

We apply the pure bending equation of the slander beam to a multi-layer bimorph PZT bending actuator. The equal strain condition at each PZT layer gives

$$\varepsilon_{PZT} = d_{31} \frac{V_{in}}{t_{PZT}} \tag{14}$$

By Eq. (14), we get the equation of a pure bending moment as following.

$$M_{PZT} = \frac{E}{\rho} \int_A y^2 dA, \tag{15}$$

where $\rho = \frac{z}{\varepsilon_x} = \frac{z}{\varepsilon_{PZT}}$. Therefore, the moment is

$$M_{PZT} = E_{PZT}\varepsilon_{PZT} \int_A zdA = E_{PZT} \frac{d_{31} V_{in}}{t_{PZT}} \int_A zdA \tag{16}$$

Using Eq. (16), the moment by the n-th PZT layer is

$$M_{PZT\_n} = E_{PZT} \frac{d_{31} V_{in}}{t_{PZT}} b \int_{\frac{2n-1}{2} t_{PZT} + nt_{PZT}}^{\frac{2n-1}{2} t_{PZT} + nt_{PZT}} zdz \tag{17}$$

Finally, the total moment in the stacked beam becomes

$$\sum_{k=1}^{n} M_{PZT\_k} = E_{PZT} \frac{d_{31} V_{in}}{t_{PZT}} b \int_{\frac{2k-1}{2} t_{stru} + (k-1) t_{PZT}}^{\frac{2k-1}{2} t_{stru} + kt_{PZT}} zdz, \tag{18}$$

where

$$\begin{aligned} I_{stru\_n} &= \frac{b}{12}(t_{stru})^3 + 2b\sum_{k=2}^{n} \left(\int_{\frac{2k-3}{2} t_{stru} + (k-1) t_{PZT}}^{\frac{2k-1}{2} t_{stru} + (k-1) t_{PZT}} z^2 dz \right) \\ I_{PZT\_n} &= 2b\sum_{k=1}^{n} \left(\int_{\frac{2k-1}{2} t_{stru} + (k-1) t_{PZT}}^{\frac{2k-1}{2} t_{stru} + kt_{PZT}} z^2 dz \right) \end{aligned} \tag{19}$$

Because of symmetry of the laminated beam, the resultant moment is

$$M = 2\sum_{k=1}^{n} M_{PZT\_k} \tag{20}$$

We use the Euler beam equation to obtain the maximum transverse deflection of beam, and then, The governing equation of the static beam is

$$M(x) = EI \frac{d^2}{dx^2} w(x) \tag{21}$$

For a cantilever beam, the force required to make the beam produce a transverse displacement, δ is given by [2]

$$F_b = \frac{3(E_{PZT} I_{PZT} + E_{stru} I_{stru})}{L^3} \delta \tag{22}$$

2.3 Dynamic analysis

To understand the dynamic properties of the multi-layer bimorph PZT actuator, we do the dynamic analysis about the PZT model. However, the PZT actuator has aperiodic non-linear property in general. We approximate the motion using a Euler beam model. After forced response analysis of a cantilever Euler beam, we get the following reponse

$$w(x,t) = \sum_{n=1}^{\infty} A_n \psi_n(x) F_{n0} e^{jwt}, \tag{23}$$

Here the modes $\psi_n(x)$, the coefficients A_n and the frequency-dependent amplitude are determined as

$$A_n = \frac{C_1}{\sin\beta_n L - \sinh\beta_n L}$$

$$\begin{aligned} \psi_n(x) = {} & (\sin\beta_n L - \sinh\beta_n L)(\sin\beta_n x - \sinh\beta_n x) \\ & + (\cos\beta_n L - \cosh\beta_n L)(\cos\beta_n x - \cosh\beta_n x) \end{aligned}$$

$$F_n(t) = -\frac{M_0 A_n V_0}{m(\lambda_n^2 - w^2)} [\varphi_n'(x_a) + \varphi_n'(x_b)]$$

3. Optimal Design of PZT Actuator and Experiments

3.1 Comparison with the theory, ANSYS analysis and experiment

When the PZT actuator is designed, some important parameters to be verified are the maximum displacement, the resultant force, and the mode frequency. In order to verify the validity of the analytical results for these parameters derived in above section, it is compared with ANSYS simulation and experimental results. Fig. 2 shows the schematic of experimental setup. The displacement is measured using the MTI-2000, The Fotonic sensor with the sensitivity of $0.02\,\mu m/mV$. In experiments, a commercial bimorph multi-layer PZT is used. The properties of PZT are shown in Table 1.

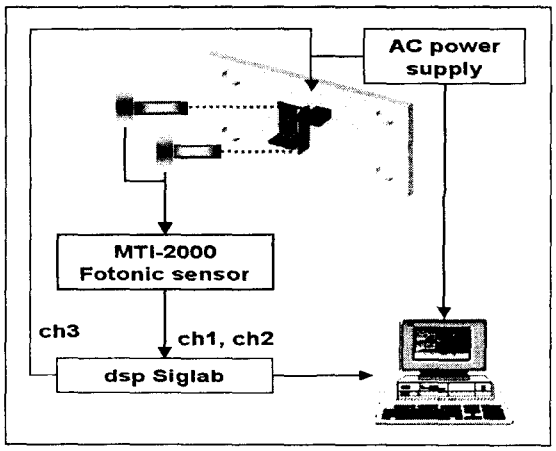

Fig. 2 Experimental setup for bimorph multilayer PZT actuator and displacement amplifier

Table 1 Properties of PZT material

Property	Values	Unit
Density	7.9×10^{3}	kg/m^{3}
Dielectric constant	3000	
Coupling factor	0.62	
d31 charge constant	-240×10^{-12}	m/V
Young's modulus	50×10^{9}	Pa

The size of the PZT actuator is $16\times6\times0.48$ mm. The material is composed of PbO (66%), ZrO_2 (21%), and TiO_2 (11%). Layer numbers is 20, and each layer thickness is $20\,\mu m$, Electrode material is Ag-Pd, and the thickness of the cover layer is $40\,\mu m$. Fig. 3 represents the hysteretic curve of the PZT actuator for periodic input between -10V ~ 10V. The maximum displacement is measured as about $37\,\mu m$. Fig. 4 shows the impulse response plot. The fundamental natural frequency of PZT actuator shown in Fig. 5 is about 20 kHz bandwidth. The PZT actuator is also analyzed by ANSYS, a commercial FEM program. The following three properties; the compliance, PZT coupling, and the relative permittivity are used in the simulation. The simulation result is shown in Fig. 6. The theoretical results by Euler or Timoshenko beam theory, ANSYS results and experimental results are summarized in Table 2.

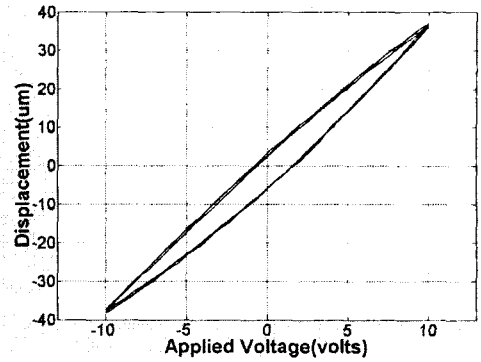

Fig. 3 Hysteresis of PZT actuator

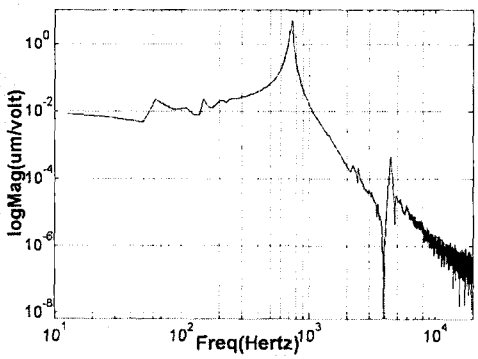

Fig. 4 Impulse spectrum graph of PZT actuator

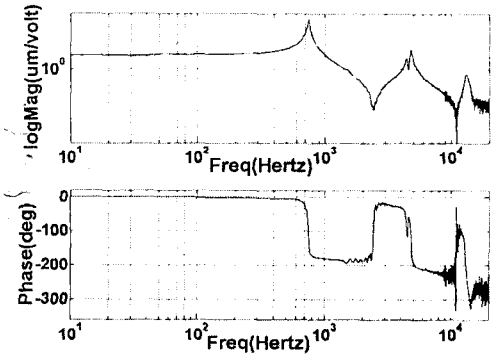

Fig. 5 FRF graph of PZT actuator

The experimental value is lower than theoretical and ANSYS results. Since the theoretical predictions agree well with experimental results, they can be used as a design guideline for the PZT actuator. The multi-layer type gives the better performance in every aspect, compared with the three-layer (PZT-electrode-PZT) type.

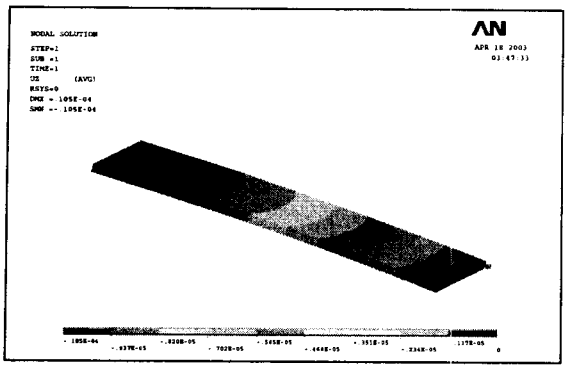

Fig. 6 Static analysis of PZT displacement by ANSYS

Table 2 Experimental/Analytical results

V=10~-10	Experiment	Experimental Equation by company	ANSYS	Theory (Euler/ Timoshenko	Three layer (same size)
Displ. [μm]	36.96 ~ -36.96	38.541 ~ -38.541	42.95	43.088 ~ -43.088	4.854 ~ -4.854
Force [N]	.	0.2178	0.2422	0.2475	0.0248
1st mode [Hz]	750	750	.	913.91	861.06
				882.98	831.92
2nd mode [Hz]	4837.5	.	.	5727.3	5396.6
				4664.6	4394.8
3rd mode [Hz]	14544	.	.	16040	15112
				13872	13070

3.2 Optimal design of multi-layer PZT

In this section, the main design parameters such as the maximum stroke, output force, and natural frequency are optimally designed using the analytical approach.

Figures 7-9 show the profiles of the displacement, force, and natural frequency at the tip position when the total thickness is constant. Here, the total thickness is the summation of PZT, electrode, and cover layers, which are 400, 40 and 40 μm, respectively. This size is the same as the multi-layer actuator used in previous analysis. Maximum force and displacement increase linearly with the layer number. Figures 10-11 represent the variations of vertical displacement and the resultant force as the layer number is increased. Contrary to the previous case where the total thickness is constant, the vertical displacement is generally decreased and the force is increased with increasing layers, if each layer

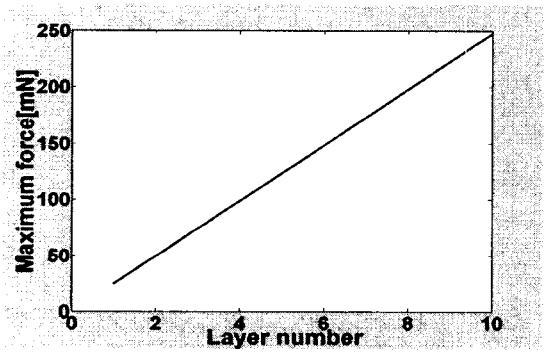

Fig. 7 Maximum force with increasing layer number (total thickness is constant)

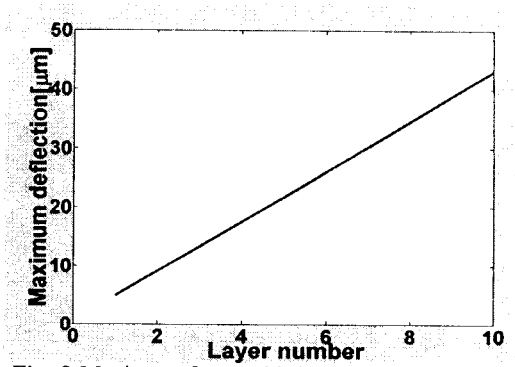

Fig. 8 Maximum force with increasing layer number (total thickness is constant)

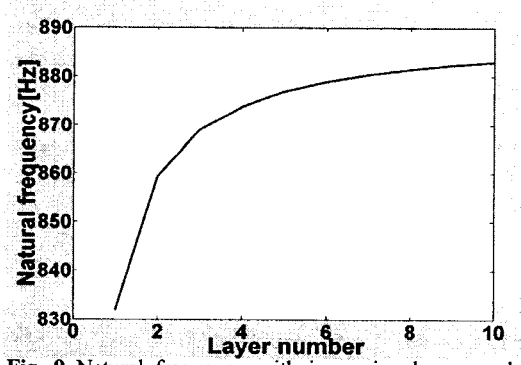

Fig. 9 Natural frequency with increasing layer number (total thickness is constant)

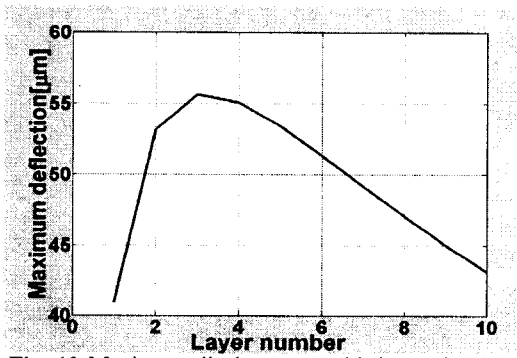

Fig. 10 Maximum displacement with increasing layer number

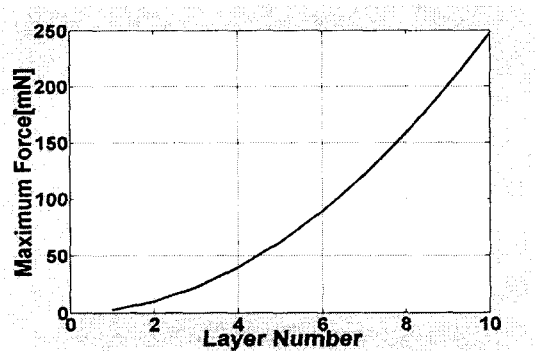

Fig. 11 Maximum resultant force with increasing layer number

has the same thickness. However, as shown in Fig. 10, when the vertical displacement is increased from one to 3 layers, and there exists a maximum stroke at a specific layer number. Our target is to design a slim PZT actuator with a large displacement stroke. The existence of the maximum displacement can be used for the optimal selection of layer number with a proper resultant force. We can determine the layer number and the thickness of PZT using above profiles to meet the target performance.

4. Analysis of a flexure hinge mechanism for PZT displacement amplifier

4.1 Basic design of the flexure hinge mechanism

The flexure hinges are widely used for systems requiring one-piece (monolithic) manufacturing. Applications include accelerometers, gyroscopes, micro-positioning translation stages, motion guides, piezoelectric actuator/motors, high accuracy alignment devices for optical fibers, missile-control devices, displacement amplifiers, scanning tunneling microscopes, high-precision cameras, robotic micro-displacement mechanisms, antennas and valves.

Functionally, an ideal flexure hinge permits the relative rotation of the rigid adjoining members, while prohibiting any other types of motion. A typical flexure hinge consists of one or two cutouts that are machined in a blank material [3]. Fig. 12 shows the geometry of a typical right circular hinge.

The flexure hinges are modeled and analyzed as Euler-bernoulli beams, which are subjected to bending produced by forces and moments. The relationship between displacement and loading at the free end 1 has the following form if normal forces at the free end 1 are zero.

$$\begin{bmatrix}\theta_z\\ \theta_y\end{bmatrix}=\begin{bmatrix}c_{11} & 0\\ 0 & c_{22}\end{bmatrix}\begin{bmatrix}M_{z_1}\\ M_{y_1}\end{bmatrix} \tag{24}$$

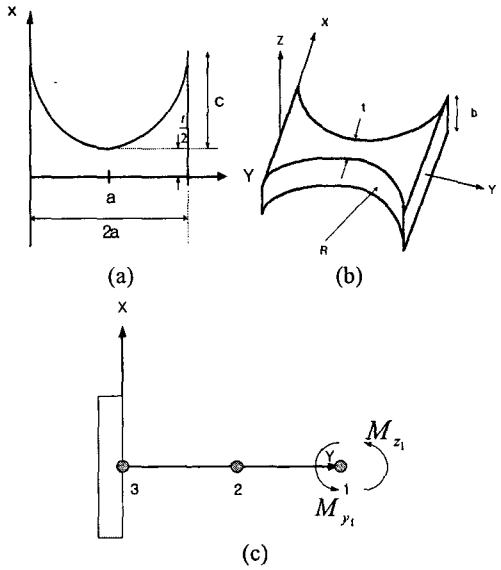

Fig. 12 Design of a right circular hinge

And the rotation angles are formulated by using Castigliano's second theorem. :

$$\theta_z=\frac{\partial U_e}{\partial M_{z_1}}\ ,\ \theta_y=\frac{\partial U_e}{\partial M_{y_1}}, \tag{25}$$

where the elastic strain energy comprises bending,

$$U_{e,z}=\frac{1}{2}\int\frac{M^2}{EI}dx\ ,\ U_{e,y}=\frac{1}{2}\int\frac{M^2}{GJ}dx \tag{26}$$

The compliance factors of equation (24) are expressed as

$$c_{11}=\frac{1}{EbI_1}\ ,\ c_{22}=\frac{1}{GbJ_1}, \tag{27}$$

where $I_1=\frac{1}{12}\int\frac{1}{t(x)^3}dx\ ,\ J_1=\int\frac{1}{t(x)^3}dx$ (28)

In the case of right circular flexure hinges, the following things are satisfied,

1. $t(x)=2R+t-[x(2R-x)]^{\frac{1}{2}}$ (29)
2. $c=a=R$
3. $\beta=\frac{t}{2c}$

Equation (29) is combined with Equations (27) and (28) to formulate the compliance equations for the circular flexure hinge, namely

$$c_{11}=\frac{12}{Ebt^2}\frac{1}{(2+\beta)^2}\left[\frac{3+4\beta+2\beta^2}{2(1+\beta)}+\frac{3(1+\beta)}{\sqrt{\beta(2+\beta)}}\tan^{-1}\sqrt{\frac{2+\beta}{\beta}}\right.$$
$$c_{22}=\frac{1}{Ebt^2}\frac{1}{(2+\beta)^2}\left[\frac{3+4\beta+2\beta^2}{2(1+\beta)}+\frac{3(1+\beta)}{\sqrt{\beta(2+\beta)}}\tan^{-1}\sqrt{\frac{2+\beta}{\beta}}\right. \tag{30}$$

4.2 Experiments of stroke amplifier model

In this paper, a hinge model is designed to use a torsion elastic deformation.(Fig. 13) The displacement amplifier displacement by this mechanism is determined by the ratio between the PZT displacement L_2 and the amplified stroke L_1. Here, a right circular hinge structure is adapted, because it shows a better performance than other types of hinges from a standpoint of precision.

The ratio of the displacement amplifier is analytically predicted to have 1/4.92. Fig. 13 shows the experimental setup to measure the flexure hinge mechanism of the stoke amplifier. As shown in Fig. 14, 15, the stroke ratio is measured about 1/4.5 experimentally, and it is observed that frequencies of vibration modes are slightly diminished. To decrease the discrepancy between the analytical and experimental result about the stroke ratio, we should consider two design factors. The first factor is that the flexural rigidity of a connection beam should be very high. And the second one to be considered is that output force at the edgy of PZT actuator should be large enough to deform the flexure hinge elastically in the torsional motion.

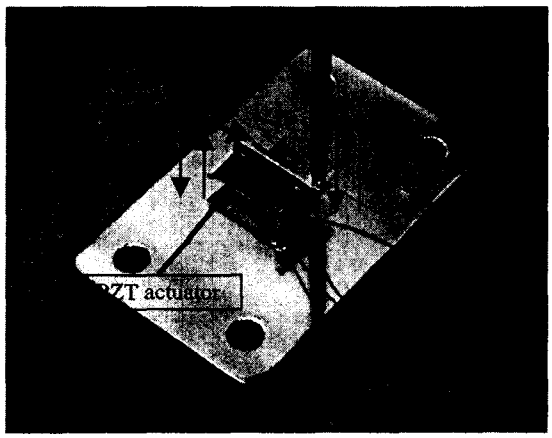

Fig. 13 flexure hinge mechanism of PZT displacement amplifier

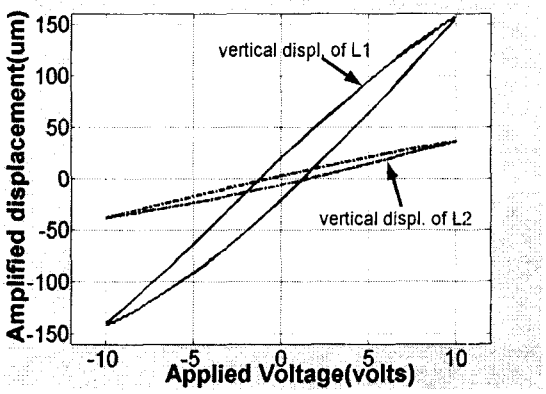

Fig. 14 Amplified motion of flexure hinge by experiment

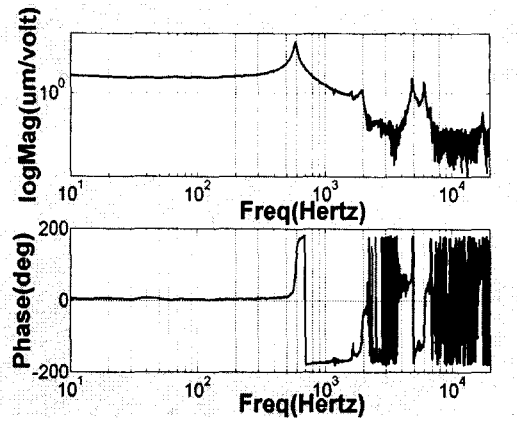

Fig. 15 Comparison of 6mm and 2.5mm of width about displacement, force, natural mode

5. Application to a pick-up actuator

Because the PZT material has a high resolution and fast response, it can be applied to an optical pick-up actuator if it is combined with a flexure hinge to extend its maximum stoke. Based on the theoretical analysis and experimental verification carried out in the paper, we plan to propose and manufacture a slim-type PZT actuator. Fig. 3 shows one of the proposed models, where the moving range is $\pm 400\mu m$ at 15V and the first natural frequency is 750 Hz. The PZT width of the suggested model is decreased to 2.5 mm (Table 3). Thus, in this case, the total thickness of a new PZT pick-up actuator is about 3 mm. The model will be experimentally verified in the future. The new slim actuator model would be an alternative of current optical pick-up actuators, because of a large stroke and fast response.

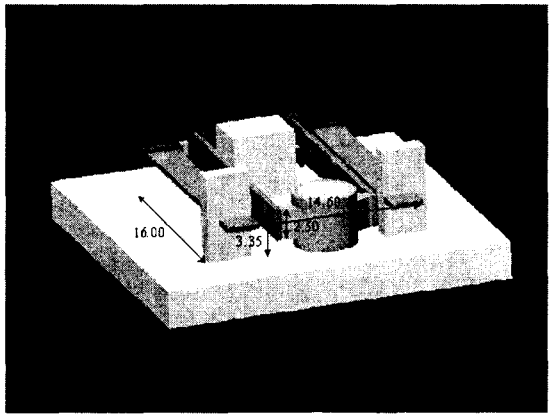

Fig. 16 Final design of a micro ODD actuator

Table 3 Comparisons of displacement, force, natural mode for two width types: 6 mm and 2.5mm

	2.5mm (10 layer)	6mm (10 layer)
Displacement[μ m]	43.088	43.088
Force [mN]	123.75	247.5
Natural frequency [Hz]	624.36	882.98

6. Conclusions

In this paper, we propose a small size pick-up actuator using a bimorph multi-layer PZT for the application of slim and small form factor ODDs. A theoretical model of a cantilever stacked beam including dynamics of the bimorph multi-layer PZT is derived and it is analytically solved to predict the natural frequency and the resultant force and displacement of the PZT actuator. A flexure hinge mechanism is used as displacement amplifier to extend the allowable stroke. The prototype of proposed model was manufactured using commercial bimorph PZTs. Experimental results agrees well with the analytical predictions. The stroke amplification ratio is measured at 4.5 in experiments. Based on the theoretical analysis and the preliminary experiments, we propose a final model for a new PZT pick-up actuator with a 2.5-mm height, which can be applicable to small form factor optical disk drives.

Acknowledgment

The work was supported by Grant No. R11-1997-042-090001-0 of the Center for Information Storage Devices designated by the Korea Science & Engineering Foundation.

References

(1) A. V. Srinivasan, Smart Structures, Cambridge University Press, pp. 15~19

(2) Bruce Geist, and Joycer R. Mclaughlin, 1998, Eigenvalue formulas for the uniform Timoshenko beam, The American Mathematical Society, Vol. 4, pp. 12-17

(3) N. Lobontiu, J. S. N. Paine, E. Garcia, M. Goldfarb, 2002, Design of symmetric conic-section flexure hinges based on closed-form compliance equations, Elsevier Science Ltd.

(4) W. Xu and T. King, Flexure hinges for piezoactuator displacement amplifiers: flexibility, accuracy, and stress consideration, Precision Engineering, Vol. 19, No. 1, pp. 4-10